Dimeric Cin8 motors have an inherent plus-end bias and weak inter-head coordination

Running title: Cin8 dimer motility

Himanshu Pandey[1], Tzu-Chen Ma[1], Eric Bonventre[2], Luke M. Rice[2], Larisa Gheber[3], and William O. Hancock[1,4 *]

[1] Department of Biomedical Engineering, Pennsylvania State University, University Park, Pennsylvania, USA
[2] Departments of Biophysics and Biochemistry, University of Texas Southwestern Medical Center, Dallas, Texas, USA
[3] Department of Chemistry, Ben-Gurion University of the Negev, Israel
[4] Department of Chemistry, Pennsylvania State University, University Park, Pennsylvania, USA

* Corresponding author:
William O. Hancock
Email: woh1@psu.edu

Abstract:
Kinesin-5 motors are bipolar tetramers that crosslink and slide antiparallel microtubules during mitotic spindle assembly. Fungal kinesin-5 motors, such as Cin8, exhibit bidirectional motility, switching between minus- and plus-end-directed stepping in response to environmental conditions; however, the molecular basis of this directional switching remains unclear. To better understand the origin of this bidirectional behavior, we investigated the motility and ATPase kinetics of two Cin8 dimers, created by fusing the motor domains to a stable coiled-coil domain from kinesin-1. To investigate the role of the proximal neck coiled-coil region in coordinating motor activity, we compared Cin8 dimers that included or lacked the first four heptads of the Cin8 neck-coil domain. By analyzing the stepping kinetics, microtubule residence times, and directional switching dynamics, we found that these Cin8 dimers move processively with a net plus-end directionality along

with undirected movements, behaviors that mimic the plus-ended motility state of wild-type Cin8. However, fast minus-ended motility seen in wild-type Cin8 tetramers was not observed in the dimers. The instantaneous velocity distributions and ATPase rates were inconsistent with the undirected movement being solely due to passive diffusion, suggesting that they reflect random bidirectional stepping. Fewer undirected movements were seen on yeast microtubules, their native physiological substrate, compared to on bovine microtubules. Replacing the Cin8 neck-coil domain with a stable coiled-coil led to faster plus-end stepping, fewer undirected movements, a reduction in the microtubule binding duration, and enhanced coupling between ATP hydrolysis and plus-end stepping. Our results suggest that the native Cin8 neck coil confers flexibility between the two motor domains that contributes to bidirectional stepping, and that sustained minus-end movement requires regions outside the motor domain.

Statement of Significance

The kinesin-5 family of motors, which contain two pairs of heads located on either end of a long stalk domain, power mitotic spindle formation by sliding antiparallel microtubules. The yeast kinesin-5, Cin8 moves to microtubule minus-ends under specific conditions, breaking the dogma that N-terminal kinesins move to microtubule plus-ends. To gain insight into how Cin8 changes its walking direction, we analyzed engineered Cin8 dimers, models of each half of full-length Cin8. The dimers step erratically, consistent with stepping in both directions, but have a plus-end bias. We find evidence that the two heads poorly coordinate, which contrasts with other kinesins, and suggest that the stepping direction may be regulated by altering the degree of inter-head coordination.

Introduction

Kinesins are a diverse family of microtubule-based motor proteins that play essential roles in intracellular transport and mitotic spindle dynamics. Canonically, kinesin directionality depends on the position of the motor domain: kinesins with N-terminal motor domains move toward the microtubule plus end, whereas C-terminal kinesins move toward the minus end (1,2). However, this paradigm is challenged by members of the kinesin-5 and kinesin-14 families of mitotic motors that exhibit bidirectional motility (3-7). During elongation of the mitotic spindle, kinesin-5 motors use their two pairs of motor domains to slide apart antiparallel microtubules, with each pair of heads moving toward microtubule plus-ends (8,9). However, fungal kinesin-5s, such as Cin8 and Kip1 from *Saccharomyces cerevisiae* and Cut7 from *Schizosaccharomyces pombe*, have also been

shown to switch to minus-end directionality under certain conditions (3-5,10). Consistent with this minus-end directionality, Cin8 localizes near the spindle pole bodies at microtubule minus ends in early mitotic cells with monopolar spindles, and this minus-end localization is proposed to enhance microtubule capture from the neighboring spindle pole bodies to set up proper spindle organization for metaphase to proceed (4,10,11). Understanding how bidirectional motility is controlled, particularly in the context of spindle assembly where precise regulation of motor protein activity is critical, remains a major challenge. Furthermore, the lack of a clear mechanism by which kinesins change their stepping direction represents a significant hole in our understanding of kinesin mechanochemistry.

In N-terminal kinesins such as kinesin-1, stepping is driven by ATP-dependent docking of the neck linker (NL) domain, a ~14-18-residue segment at the C-terminal of the motor domain (12). Upon ATP binding and hydrolysis, the neck linker transitions from an undocked, unstructured conformation to a docked beta-sheet conformation that is stabilized along the catalytic core by the N-terminal 'cover strand' (13-15). This conformational change positions the partner (tethered) head toward the microtubule plus end where it then binds to complete a plus-end directed (forward) step (13,16). In the resulting two-head bound state, the now trailing head has its neck linker docked forward, while the leading head has its neck linker stretched backward, and this inter-head tension transmitted through the neck domains is thought to coordinate the ATPase cycles of the two heads to ensure processive, hand-over-hand stepping (16-19). Consistent with this, increasing the length and flexibility of the neck linker domain has been shown to disrupt head-head coordination and reduce processivity (18,20-22).

A dominant theme that emerges from Cin8 work to date is that perturbations that enhance microtubule affinity bias the motor toward slow plus-end motility, whereas perturbations that reduce the microtubule affinity tend to bias the motor toward fast minus-end directionality. For instance, motor clustering and crosslinking of antiparallel microtubules by Cin8 bias it toward plus-end-directed motility (3,23). In contrast, increasing the ionic strength or deleting the N-terminal extension, loop-8, or the C-terminal tail, all of which can interact with microtubules, bias the motor toward minus-end directionality (3,4,24-26). The underlying mechanism, however, remains unexplained. A recent model proposes that Cin8 inherently steps in both directions, with minus-end stepping dominating at zero load but having a stronger dependence on load such that plus-end stepping dominates under load (23). An alternative model for the related fungal kinesin-5, Cut7, posits that stepping is inherently minus-end directed and crowding on the microtubule surface promotes plus-end stepping by a steric blocking mechanism (11).

There is also evidence that directionality of Cin8 is regulated allosterically by regions outside the motor domain such as the tail or the N-terminal non-motor region (24-26).

In the present study, we investigated the role of inter-head coordination in the bidirectional stepping of dimeric Cin8. We hypothesized that directional switching is enabled by loose mechanical coupling between the motor domains. To test this, we used the stable coiled-coil of kinesin-1 to dimerize Cin8 motor domains with and without their native proximal neck-coil dimerization domain. We compared the stepping speed and directionality on both bovine and yeast microtubules and analyzed the undirected movements to determine the relative contributions of Brownian diffusion and ATP-driven stepping. Our results demonstrate that Cin8 dimers exhibit slow net plus-end motility along with undirected movements, and that flexibility in the proximal neck-coil reduces inter-head coordination and leads to partial uncoupling between ATP hydrolysis and plus-end directed stepping. These findings support a model in which loose mechanical coordination between motor heads, modulated by structural elements of the neck region, plays a critical role in enabling bidirectional motility in fungal kinesin-5.

Methods

Protein Constructs

Plasmids to express Cin8 variants were generated using standard PCR and Gibson assembly and verified by DNA sequencing. All constructs are dimers comprising the *S. cerevisiae* Cin8 motor and neck domains (residues 39–530 for Cin8Kin and 39–558 for $Cin8_{+28NC}$Kin), fused to the Drosophila KHC neck-coil and dimerization coiled-coil domain (residues 345–560; Fig. 1A). Constructs were made by inserting the Cin8 motor domains into the K560-AviN plasmid described previously (27). All constructs begin at Cin8 residue 39 and include a C-terminal AviTag™ and His_6 tag for purification.

Purification and Quantification

Bacterial expression procedures were adapted from previously described protocol (25,27). Briefly, constructs were expressed in E. coli BL21-CodonPlus (DE3) grown in 1 L of terrific broth, in-house. 24 mg/l of biotin were added along with the isopropyl 1-thio-β-d-galactopyranoside (IPTG) at the time of induction, followed by nickel gravity column chromatography purification with an 50 mM HEPES based elution buffer containing 2 μM mant-ADP along with 0.25 mM TCEP, 5% glycerol, 500 mM KCl, 10 mM $MgCl_2$, 0.01% Triton X-100, pH 7.2. The elution fraction containing motors were supplemented with 10% (w/v) sucrose and 2 mM DTT, flash-frozen and stored at -80 °C. The active motor concentration

141 was determined by measuring the total mant-ADP concentration (356 nm excitation/450
142 nm emission) in a Shimadzu 3000 spectrofluorometer and correcting for the free mant-
143 ADP, and using a fluorescence enhancement factor of 1.8 for motor-bound mant-ADP (28).
144 Stock active dimeric motor concentrations were in the range of 1–10 μM dimer.

145 **Gliding assay**

146 Flow chambers were assembled and motors adhered to the surface by flowing in 20 μg/ml
147 NeutrAvidin followed by C-terminal biotinylated motors. Taxol-stabilized microtubules were
148 then added to the flow cell in motility buffer (BRB80 adjusted to pH 7.2, 1 mM ATP, 10 μM
149 Taxol, 2 mM $MgCl_2$, 5 mM DTT, and 2 mg/ml casein, 0.5 mg/ml BSA). Microtubule
150 movements were monitored with the microscopy setup described for the single-molecule
151 motility assay and recorded at 5 fps. Microtubule velocities were measured by creating
152 kymographs along the MT path using ImageJ-Fiji software and measuring the slope. Periods
153 when microtubules paused or stopped moving were not included in the velocity analysis.

154 **Single-molecule motility assay**

155 Motility assays were performed on a Nikon TE2000 TIRF microscope equipped with
156 interference reflection microscopy, at room temperature, as described previously (29,30).
157 Dimeric Cin8 motors were labeled with streptavidin-labeled Quantum dots (Qdot 525;
158 Thermo Fisher) through the C-terminal AviTagTM bound biotin. For labelling, 100 nM
159 dimeric motors were mixed with Qdots at 1:5 ratio of motor:Qdots and incubated in ice for
160 20 min, such that each dimeric motor molecule is labeled with one Qdot. Flow cells were
161 functionalized by flowing in 0.5 mg/ml casein, followed by full-length rigor kinesin (27) in
162 the motility buffer (BRB80 adjusted to pH 7.2, 1 mM ATP/ADP, 10 μM Taxol, 2 mM $MgCl_2$, 5
163 mM DTT, and 2 mg/ml casein, 1 mg/ml BSA, 10 mM glucose, 100 μg/ml glucose oxidase, 80
164 μg/ml catalase 40, 10 mM phosphocreatine, and 50 μg/ml creatine phosphokinase). Taxol-
165 stabilized microtubules, polymerized from bovine or yeast tubulin, were then introduced
166 into the flow cell, where they attached to surface-immobilized rigor kinesin. Subsequently,
167 Qdot labeled motors were introduced and imaged. To accurately measure run times,
168 motors were introduced into the flow cell immediately upon initiating image acquisition,
169 ensuring that no motors were bound prior to the start of imaging. Cin8 motility on surface-
170 attached microtubules was recorded at either 20 fps or 5 fps and analyzed using FIESTA
171 software (31) to determine velocity and run durations. When measuring run durations,
172 motors that landed during the final 20% of the total acquisition time were excluded from
173 the analysis to prevent censoring by termination of the video. Microtubule polarities were
174 determined by flushing in fluorescent KIF1A at the end of the experiment (28).

175 **Data analysis**

Single-molecule tracking movies of Cin8 dimers were analyzed with FIESTA (31) to generate displacement along microtubule versus time trajectories. From the tracked traces two types of motility behaviors were evident: directed motility traces where motors move processively towards plus ends of microtubules, and undirected traces, which we defined as those with average velocities < 20 nm/s and net displacements < 1 μm (the majority of which were < 0.5 μm). For mean-squared displacement (MSD) analysis, we calculated the squared displacement during each time lag (τ) for each tracked particle and averaged the squared displacements over all particles. To estimate the diffusion coefficients (D) we fit MSD data with $v^2\tau^2 + 2D\tau + s^2$, where v is mean velocity obtained from the 5 s instantaneous velocity distribution and s set to 10 nm based on the point spread function measurement error in FIESTA. For Gaussian Mixture Model fitting, we used Matlab built-in function "fitgmdist" to fit the PDF distribution of 5-s instantaneous velocities with 3 Gaussian functions. The maximum iteration was set to 1000 to ensure convergence of the fit. All the fitting and plotting were performed using Matlab. Kymographs were generated using ImageJ-FIJI (32).

Steady state ATPase assay

Cin8 ATPase activity at varying [Mt] was quantified by an enzyme-coupled assay following a protocol adapted from Huang and Hackney (28,33). BRB80 buffer supplemented with 1 mM Mg-ATP, 2 mm phosphoenolpyruvate, 1 mm $MgCl_2$, 0.2 mg/ml casein, 10 μM Taxol, 0.25 mM NADH, and 1.5% volume % of Pyruvate Kinase/Lactate dehydrogenase (Sigma P-0294) was used for ATPase assays at 21 °C. Dimeric motor concentrations between 50 and 100 nM were used. NADH absorbance at 340 nm was measured over time on a Molecular Devices FlexStation3 microplate reader, converted to an ATPase rate by linear fit to regions of steady-state absorbance decrease, and divided by the active dimer-motor concentration to give the total hydrolysis cycle rate. k_{cat} and K_M (MT) were determined from the fit to a Michaelis-Menten equation of ATP turnover rates at various microtubule concentrations. Mean ± SD values were obtained from five independent assays for each Cin8 variant with motors from at least two different purification preparations.

Simulations

Cin8 stepping simulations used a Gillespie stochastic stepping model based on an algorithm developed in previous work (34,35). Plus-end directed stepping was the only reaction considered, with the unloaded stepping rate, $k^0_{forward}$ taken from the mean velocity on yeast microtubules, assuming an 8 nm step size. To model diffusion, a diffusive term was added to each step based on sampling from a normal distribution with mean of zero and standard deviation $\sigma = \sqrt{2D\tau}$, where D is the chosen diffusion coefficient and τ is the

211 transition time for that step. All simulations were run 1000 times, and each run was
212 recorded for 50 seconds.

213

214 # Results

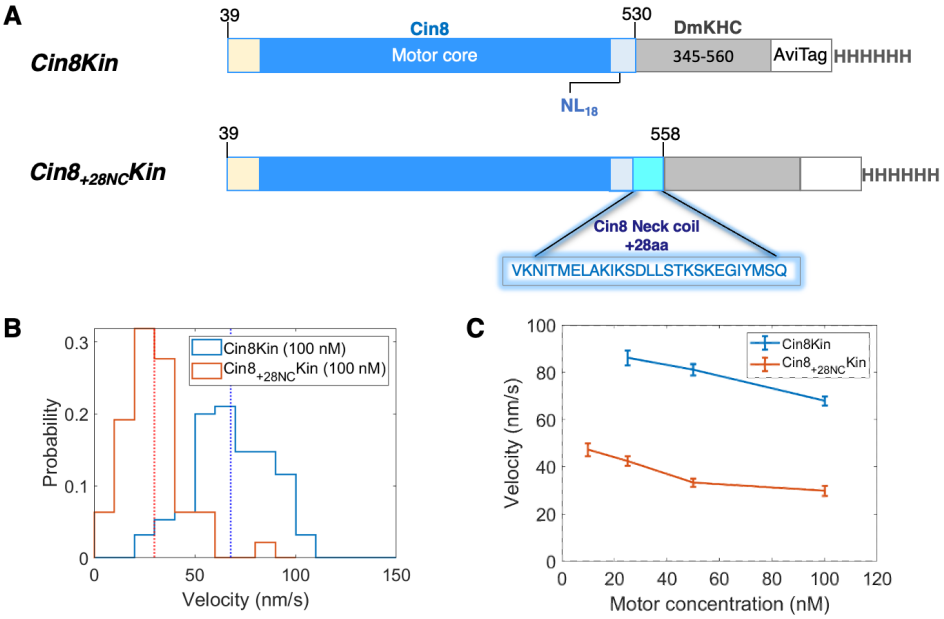

215

216 **Fig. 1: Design and microtubule gliding velocities of dimeric Cin8 constructs. (A)** Domain
217 organization of Cin8 constructs used in this study. The Cin8 catalytic motor domain (residues 76–
218 512, blue) is flanked by the N-terminal non-motor region (residues 39–75, yellow) and the C-
219 terminal neck-linker, NL_{18} (residues 513–530, light blue). In Cin8Kin, the Kinesin-1 neck-coil and
220 dimerization domain (residues 345–560, gray) are fused downstream of the Cin8 head, followed by
221 a C-terminal Avi Tag (white) and His_6 tag. The $Cin8_{+28NC}Kin$ construct includes additional 28 residues
222 from the Cin8 neck coil (residues 531–558, cyan), inserted between the Cin8 head and the Kinesin-
223 1 dimerization domain. Diagrams are not to scale **(B)** Distribution of microtubule gliding velocities
224 for both motors with 100 nM motors introduced into flow cell. **(C)** Microtubule gliding velocities at
225 varying motor concentrations in the flow cell.

226

227 **Cin8 dimers are plus-end steppers in microtubule gliding assays**

228 To investigate the role of inter-head tension in the directional switching and motility of
229 Cin8, we used a simplified dimeric construct lacking the second pair of motor domains, the
230 tetrameric stalk, and the native tail. To improve solubility, the first 38 amino acids of the
231 unstructured N-terminal domain were deleted. Stable dimers were created by fusing the
232 Cin8 motor domain (amino acids 39–530) to the neck coil and coiled-coil-1 of *Drosophila*

233 kinesin-1 (amino acids 345-560), followed by a biotinylation tag and His_6tag (Fig. 1A). This
234 dimerization strategy has been used successfully for motors from the kinesin-1, 2, 3, 5, and
235 7 families and thus allows for direct comparison to previous work (18,28,36-38). The first
236 dimeric construct, Cin8Kin, consists of the Cin8 catalytic core and 18-residue neck linker
237 domain (amino acids 39-530) fused to the kinesin-1 dimerization domain. This construct is
238 similar to one used previously in multimotor gliding assays (25), but lacks N-terminal
239 residues 1-38 and four C-term residues compared to a Cin8Kin construct (residues 1-534)
240 used previously in single-molecule assays (24).

241 Processive kinesin stepping requires a mechanical connection between the two motor
242 domains, which is achieved through dimerization of the neck-coil domain. In contrast to
243 kinesin-1 (39), the stability of the proximal neck-coil domain of Cin8 is not known. Coiled-
244 coil prediction analyses indicate that the proximal neck coil of Cin8 is less stable than
245 kinesin-1, as evidenced by lower coiled-coil stabilization scores and a reduced number of
246 stabilizing interactions (Fig. S1). Because the inter-head tension that coordinates the hand-
247 over-hand stepping in processive kinesins relies on the proximal neck-coil remaining tightly
248 dimerized, we designed a second construct, $Cin8_{+28NC}$Kin, that included the first four
249 heptads (28-residues) of the native Cin8 neck coil. These constructs were bacterially
250 expressed and purified following standard procedures.

251 To confirm that the Cin8 dimers are functional, we tested their activity in multi-motor
252 microtubule gliding assays. When biotinylated motors (100 nM solution concentration)
253 were adsorbed to a neutravidin-coated coverslip, $Cin8_{+28NC}$Kin and Cin8Kin steadily drove
254 bovine microtubules in a unidirectional plus-ended manner with no evidence of directional
255 switching. Notably, the $Cin8_{+28NC}$Kin construct exhibited a microtubule gliding velocity
256 approximately half that of Cin8Kin, providing evidence that the native Cin8 neck-coil lacks
257 the stability of kinesin-1 (Fig. 1B). Previous work using full-length tetrameric Cin8 showed
258 that microtubule gliding switched to minus-end directionality as the surface motor density
259 was decreased (4). To test this, we decreased the motor concentration in the gliding assay
260 and found no change in directionality. Instead, there was a slight increase in plus-end
261 velocity for both motors at reduced motor densities (Fig. 1C). Thus, in multi-motor assays,
262 Cin8 dimers displayed plus-end directionality, and dimerizing the heads just distal to their
263 neck linker doubled the gliding speed compared to dimers that retained the first four
264 heptads of the native Cin8 neck-coil.

265

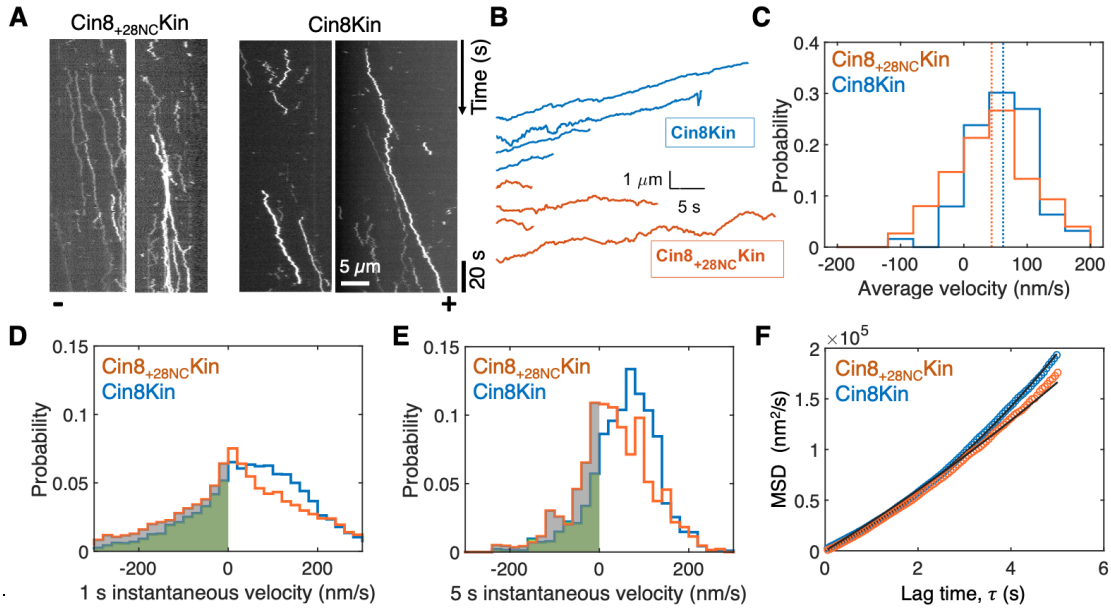

Fig. 2: Single-molecule Cin8 dimer motility on bovine microtubules. Representative **(A)** kymographs and **(B)** displacement versus time traces for Cin8$_{+28NC}$Kin (orange) and Cin8Kin (blue) in the presence of 1 mM ATP on surface-immobilized bovine microtubules. Motors were labeled with quantum dots and movies acquired at 5 frames/s. Microtubule polarities, determined by introducing fluorescent KIF1A at the end of the experiment (Fig. S2), are marked at the bottom of kymograph. **(C)** Distribution of whole trace velocities for Cin8$_{+28NC}$Kin and Cin8Kin. Mean velocities were 43.8 ± 7.3 nm/s for Cin8$_{+28NC}$Kin and 62.1 ± 6.4 nm/s for Cin8Kin (mean ± SEM for n= 75 and 63, respectively). **(D)** 1 s and **(E)** 5 s instantaneous velocity distributions for Cin8$_{+28NC}$Kin and Cin8Kin. Average velocities from the 5 s velocity distributions were 32.9 ± 6.2 nm/s for Cin8$_{+28NC}$Kin and 58.6 ± 6.3 nm/s for Cin8Kin (mean ± SEM for N = 516 and 148 independent 5 s windows, respectively). Gray (Cin8$_{+28NC}$Kin) and green (Cin8Kin) shaded areas represent minus-end directed velocity segments. **(F)** Mean squared displacement (MSD) analysis in ATP. Data at varying lag time (τ) were fit to MSD = $v^2\tau^2+2D\tau$ (black lines), with velocities (v) fixed at 32.9 nm/s (Cin8$_{+28NC}$Kin) and 58.6 nm/s (Cin8Kin). Apparent diffusion coefficients (D) were 14338 ± 172 nm^2/s and 10921 ± 40 nm^2/s, respectively (fit ± 95% CI). Fit to MSD = $a\tau^{\alpha} + b$ gave α of 1.29 for Cin8$_{+28NC}$Kin and 1.38 for Cin8Kin (Table S1).

Single Cin8 dimers move processively with net plus-end directionality

To investigate the speed and directionality of individual Cin8 dimers, we labeled the motors with streptavidin-coated quantum dots and observed their movements along immobilized microtubules polymerized from bovine brain tubulin (Fig. 2A & B). Consistent with the microtubule gliding assays, both Cin8 constructs displayed net plus-end directed movement (Fig. 2A-C & S2), with average trace velocities of 43.8 ± 7.3 nm/s for Cin8$_{+28NC}$Kin

290 and 62.1 ± 6.4 nm/s for Cin8Kin (mean ± SEM; Fig. 2C). However, in contrast to the smooth
291 movements in the multi-motor gliding assay, there were durations of undirected
292 movement, fluctuations in velocity during plus-end directed segments, and frequent short
293 segments with minus-end directionality (Fig. 2A & B). To more comprehensively compare
294 the single-molecule motility, we calculated instantaneous velocities for every trace using a
295 1 s or 5 s window for both motors and plotted the resulting instantaneous velocity
296 distributions (Fig. 2D & E). The 1 s and 5 s results were similar, but due to the long tails in
297 the 1 s distributions we focused our analysis on the 5 s distributions. Both variants had a
298 clear plus-end bias, with Cin8Kin having a distinct peak around ~100 nm/s and Cin8$_{+28NC}$Kin
299 having a broader distribution that was centered closer to zero. Notably, even with this
300 relatively long 5 s window, 33% of Cin8$_{+28NC}$Kin and 18% of Cin8Kin segments were minus-
301 end directed (Fig. 2E, shaded region), consistent with the considerable undirected
302 movements seen in the raw traces (Fig. 2A&B).

303 As an alternative way to quantify the degree of undirected motility, we carried out a mean
304 squared displacement (MSD) analysis using the mean velocity from the instantaneous
305 velocity distributions along with a diffusive term (Fig. 2F). Consistent with the wider
306 instantaneous velocity distribution, the apparent 1D diffusion coefficient was 14338 ± 172
307 nm^2/s for Cin8$_{+28NC}$Kin and 10921 ± 40 nm^2/s for Cin8Kin (fit ± 95% confidence interval, CI).
308 Fitting to a model MSD = $a\tau^{\alpha} + b$, where $\alpha = 1$ denotes pure diffusion and $\alpha = 2$ denotes
309 processive directional movement gave α of 1.29 for Cin8$_{+28NC}$Kin and 1.38 for Cin8Kin (Table
310 S1). Thus, consistent with its broader velocity distribution, Cin8$_{+28NC}$Kin displayed more
311 diffusion-like undirected movement than Cin8Kin.

312 Previous work on tetrameric Cin8 found that weakening motor-microtubule interactions by
313 increasing the buffer ionic strength resulted in a shift to minus-end directionality (3,4,23).
314 To test whether increasing ionic strength caused a similar directionality shift for Cin8
315 dimers, we repeated the experiments in BRB80 buffer supplemented with 110 mM KCl. In
316 contrast to tetramers, clear net plus-end motility of Cin8$_{+28NC}$Kin and Cin8Kin dimers was
317 retained in the presence of added KCl, with slightly higher whole trace velocities of 47.3 ±
318 7.0 and 84.1 ± 7.6 nm/s, respectively (mean ± SEM) (Fig. S3). Thus, engineered Cin8 dimers
319 display more inherent plus-end bias than native tetramers.

320

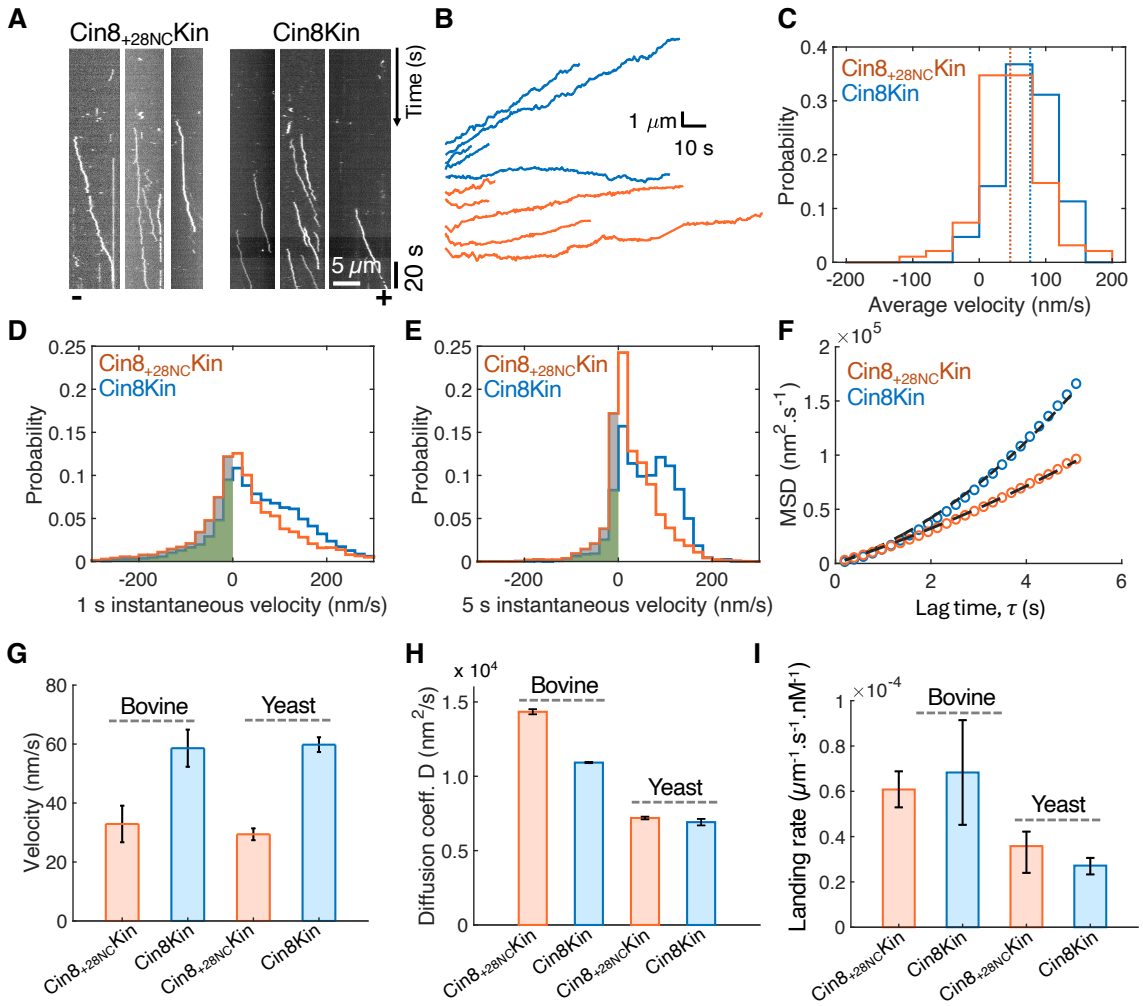

Fig. 3: Cin8 dimer motility on yeast microtubules. (A) Representative kymographs and (**B)** displacement versus time traces for Cin8$_{+28NC}$Kin (orange) and Cin8Kin (blue) motility in the presence of 1 mM ATP on yeast microtubules. Microtubule polarities are marked at the bottom of kymographs. **(C)** Distribution of whole trace velocities, with mean velocities 46.7 ± 4.4 for Cin8$_{+28NC}$Kin and 76.6 ± 4.2 nm/s for Cin8Kin (mean ± SEM for 95 and 106 traces). **(D)** 1 s and **(E)** 5 s instantaneous velocity distributions. Gray (Cin8$_{+28NC}$Kin) and green (Cin8Kin) shaded areas represent minus-end directed velocity segments. Average velocities from the 5 s velocity distributions were 29.4 ± 2.0 nm/s for Cin8$_{+28NC}$Kin and 59.8 ± 2.5 nm/s for Cin8Kin (mean ± SEM for N = 726 and 179 independent 5 s windows, respectively). **(F)** Mean squared displacement (MSD) analysis in ATP. Data were fit to, MSD = $v^2\tau^2+2D\tau$ (black lines), with velocities taken from Fig. 3E, yielding diffusion coefficients of 7194 ± 94 nm^2/s and 6915 ± 220 nm^2/s, respectively (fit ± 95% CI). Fit to MSD = $a\tau^{\alpha} + b$ yielded α of 1.29 for Cin8$_{+28NC}$Kin and 1.64 for Cin8Kin (Table S1). **(G)** Comparison of velocities (summarized from Figs. 2E & 3E). **(H)** Comparison of diffusion coefficients and **(I)** motor landing rates for Cin8$_{+28NC}$Kin (0.06 ± 0.007 and 0.036 ± 0.006 μm^{-1} s^{-1} nM^{-1} for bovine vs yeast, respectively; mean ± SEM) and Cin8Kin (0.068 ± 0.02 and 0.027 ± 0.002 μm^{-1} s^{-1} nM^{-1} for

337 bovine vs yeast, respectively; mean ± SEM) on bovine and yeast microtubules (2 and 3 fields,
338 respectively).

339

340 **Cin8 dimers move more directionally on yeast microtubules**

341 To test the role of the microtubule track on Cin8 motility, we carried out single-molecule
342 assays using recombinant *S. cerevisiae* tubulin, matching the species of the *S. cerevisiae*
343 Cin8. To the best of our knowledge, only one previous study investigated the motility of
344 Cin8 on yeast microtubule in vitro, and that study used full-length Cin8 tetramers from
345 yeast lysates (40). On yeast microtubules, both Cin8 dimer constructs exhibited similar net
346 plus-end directed motility as on bovine microtubules, though by visual inspection there
347 were fewer fluctuations in directionality on the yeast microtubules (Fig. 3A&B; see also Fig.
348 S4A). To quantify this undirected movement, we compared the fraction of traces that
349 showed clear processive movements, defined as traces with average velocities >20 nm/s
350 and net displacements >1 µm. Compared to bovine microtubules, the overall fraction of
351 directed traces on yeast microtubules increased from 28% to 41% for Cin8$_{+28NC}$Kin and
352 from 26% to 68% for Cin8Kin (Fig. S4B). Similar to the bovine microtubules, replacing the
353 proximal neck-coil of Cin8 with the stable kinesin-1 dimerization domain increased the
354 mean trace velocity from 46.7 ± 4.4 nm/s for Cin8$_{+28NC}$Kin to 76.6 ± 4.2 nm/s for Cin8Kin
355 (mean ± SEM for 95 and 106 traces, respectively; Fig. 3C).

356 To quantify the relative proportions of directional and nondirectional movements on yeast
357 microtubules, we carried out instantaneous velocity and mean squared displacement
358 analyses. The instantaneous velocity analyses (Fig. 3D&E) revealed clear minus-end
359 movements, particularly for Cin8$_{+28NC}$Kin – from the 5 second instantaneous velocity
360 distributions, 26.8% of segments were minus-end directed for Cin8$_{+28NC}$Kin versus 13.7%
361 for Cin8Kin (shaded regions). Cin8$_{+28NC}$Kin also had a broader instantaneous velocity
362 distribution than Cin8Kin with a standard deviation of 53.9 nm/s versus 33.4 nm/s,
363 respectively (Fig. 3E). From the MSD analysis (Fig. 3F&H), the apparent diffusion constants
364 on yeast microtubules were also similar to one another (7194 ± 94 nm^2/s for Cin8$_{+28NC}$Kin
365 and 6915 ± 220 nm^2/s for Cin8Kin); however fitting to MSD = aτ^{α} + b gave α of 1.29 for
366 Cin8$_{+28NC}$Kin and 1.64 for Cin8Kin, consistent with a greater degree of processive
367 movement for Cin8Kin (Table S1). Interestingly, despite the shift toward more consistent
368 plus-ended motility on yeast microtubules, motor landing rates on yeast microtubules
369 were lower than on bovine microtubules (Fig. 3I). Overall, on yeast microtubules the mean
370 velocities for each motor matched those on bovine microtubules (Fig. 3G); however, there

was less undirected motility for both motors on yeast microtubules, which revealed more clearly the greater degree of undirected motility of Cin8$_{+28NC}$Kin relative to Cin8Kin.

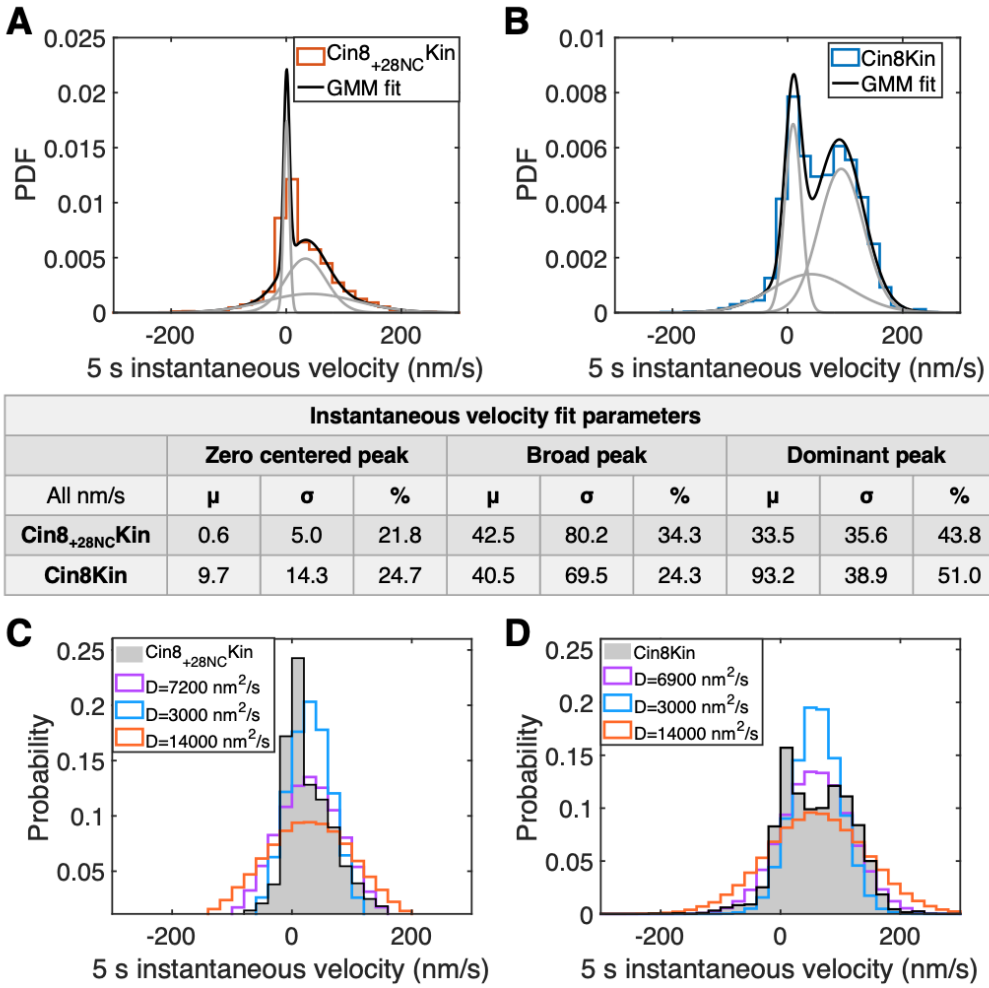

Instantaneous velocity fit parameters									
	Zero centered peak			Broad peak			Dominant peak		
All nm/s	μ	σ	%	μ	σ	%	μ	σ	%
Cin8$_{+28NC}$Kin	0.6	5.0	21.8	42.5	80.2	34.3	33.5	35.6	43.8
Cin8Kin	9.7	14.3	24.7	40.5	69.5	24.3	93.2	38.9	51.0

Figure 4. Separating diffusion from bidirectional stepping. (A and B) Gaussian Mixture Model analysis of 5 s instantaneous velocity distributions. Velocity distributions on yeast microtubules (from Fig. 3E) were fit by three Gaussians (gray lines), with values given in table. (**C and D**) Comparison of experimental results with simulations of a motor with a unidirectional velocity plus random diffusion. Motor velocities were taken from mean of instantaneous velocity distributions in Fig. 3E. Initial diffusion constants (purple line) were taken from MSD analysis in Fig. 3F and varied up and down by two-fold. The experimental velocity distribution from Fig. 3D&E are shown in gray, whereas the distributions shown by cyan, purple and magenta represent simulated data with diffusion coefficients values given in figure inset. In the table, μ, σ and % represent mean, standard deviation, and weight of each Gaussian distribution, respectively.

Instantaneous velocity distributions are not consistent with simple diffusion

To gain further insight into the degree to which the undirected movements reflected bidirectional stepping versus thermally driven diffusion, we analyzed the instantaneous velocity distributions using a Gaussian Mixture Model. We first asked whether the velocity distributions on yeast microtubules could be decomposed into sum of two normal distributions representing processive stepping and undirected diffusion or bidirectional stepping. A sum of two Gaussian did not fit the data well (Fig. S5). Instead, the velocity distributions for both Cin8Kin and Cin8$_{+28NC}$Kin were well fit by the sum of three Gaussians (Fig. 4A&B). For each variant there was a principal mode (dominant peak) corresponding to plus-ended stepping; there was a narrow mode centered around zero (zero-centered peak), and there was a third mode with a very wide distribution (broad peak). The first difference between the two dimers was that the dominant velocity peak, which accounted for approximately 50% of the total distribution in both cases, exhibited markedly different mean velocities: 33.5 nm/s for Cin8$_{+28NC}$Kin compared to 93.2 nm/s for Cin8Kin. The second difference was the width of the broad velocity peak, with Cin8$_{+28NC}$Kin having a larger standard deviation (80.2 nm/s) than Cin8Kin (69.5 nm/s) and accounting for a greater proportion of the distribution (34% versus 24%). Together, these fits reiterate the observation that Cin8$_{+28NC}$Kin exhibited greater stepping variability and reduced net plus-end velocity than Cin8Kin. In principle, the narrow modes centered around zero could reflect unbiased thermal diffusion while the broad peaks could represent bidirectional stepping with a plus-end bias. However, these data alone are not sufficient to support that interpretation. In sum, the presence of three modes in the velocity distribution argues against model consisting only of plus-end stepping and simple diffusion.

As a second test of whether simple diffusion can account for the observed undirected movements, we carried out stochastic simulations of Cin8 motility that included motor stepping and diffusion. We took the stepping rate from the mean velocity of the 5 s velocity distribution for each motor and added a diffusive term ($\langle x(t)\rangle^2 = 2Dt$), where D is the apparent diffusion constant. We generated simulated motility traces and analyzed them in the same manner as the experimental data to generate a 5 second instantaneous velocity distribution (Fig. 4 C&D). When we chose a value of D from the MSD analysis in ATP (7194 nm^2/s and 6915 nm^2/s), the resulting distributions were wider than the experimental and they also failed to capture the height of the peaks (cyan curves in Fig. 4 C&D). For both variants, a smaller D was able to reproduce the tails of the distribution, but the peaks were not aligned with the experimental peaks (purple curves in Fig. 4 C&D)). Finally, a larger D failed to capture either the peak or the tails of the distribution (magenta curves in Fig. 4 C&D). The failure of a simple plus-end directed stepping plus diffusion model to recapitulate the experimental data, together with the finding that the distributions were fit

424 by three Gaussians (Fig. 4 A&B) strongly suggest that the undirected movements result
425 from bidirectional stepping and not solely due to thermally driven diffusion of the motors.

426

427

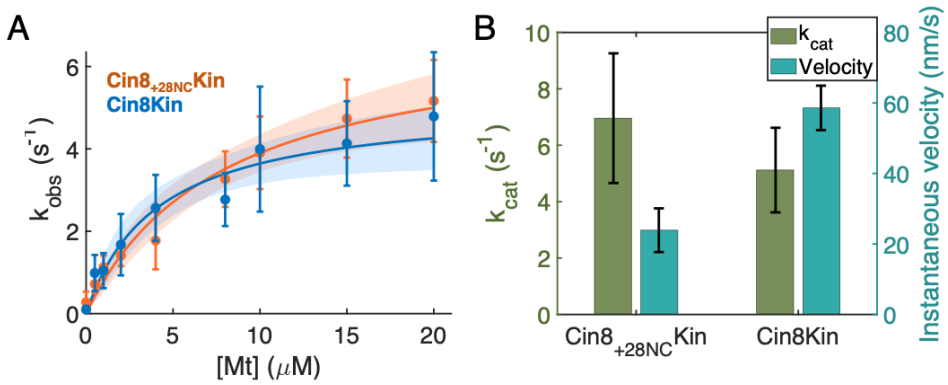

	k_{cat} (s^{-1})	K_M (μM)
Cin8$_{+28NC}$Kin	6.9 ± 2.3	7.8 ± 5.4
Cin8Kin	5.1 ± 1.5	4.0 ± 3.1

428

429 **Fig. 5. ATP turnover kinetics and corresponding stepping velocities. (A)** Microtubule-stimulated
430 ATP hydrolysis of Cin8 dimers in BRB80 buffer at various bovine microtubule concentrations (n = 5
431 trials per point). Data were fit to the Michaelis-Menten equation, using 1/SEM weighing for each
432 point, to obtain the k_{cat} and a K_m (± 95% CI) presented in the table. Shaded area represents fit ± 95%
433 CI. **(B)** Comparison of k_{cat} (fit ± 95% CI; left axis, green) to the 5 s mean instantaneous velocity
434 (mean ± SEM; right axis, blue) for Cin8$_{+28NC}$Kin and Cin8Kin (from Fig. 2D).
435

436 **ATPase kinetics indicate that flexibility of the Cin8 neck coil diminishes**
437 **mechanochemical coupling**

438 Understanding how ATP hydrolysis is coupled to mechanical stepping is central to
439 understanding the kinesin stepping mechanism. For kinesin-1, the stepping rate (k_{step})
440 matches the ATP hydrolysis rate (k_{cat}), consistent with the motor hydrolyzing one ATP per
441 step, defined as tight mechanochemical coupling (41,42). In our single-molecule assays,
442 both Cin8 dimers showed net plus-end directed processive motility along with undirected
443 fluctuations, which in principle could result from either pure diffusion with no ATP
444 hydrolysis (the consensus model for processive monomeric KIF1A motors (43)) or from
445 bidirectional stepping (with each step consuming one ATP). Cin8$_{+28NC}$Kin, which contains its
446 native proximal neck-coil domain had a slower net plus-end velocity and more undirected
447 movement. If this undirected movement was simply diffusion, the Cin8$_{+28NC}$Kin ATPase rate
448 would be expected to be lower than that of Cin8Kin, reflecting the time the motor spends in

a diffusive state. In contrast, if the greater undirected movement of Cin8$_{+28NC}$Kin was due to bidirectional stepping, the ATPase rate would be expected to be higher than Cin8Kin. To examine the degree of mechanochemical coupling for the two Cin8 dimers, we measured the microtubule-stimulated ATPase rates at varying concentrations of bovine microtubules using an NADH-coupled assay (Fig. 5A). Cin8Kin had a mean plus-end velocity of 58.6 nm/s on bovine microtubules (Fig. 2E), corresponding to 7 steps/s, and the measured k_{cat} was 5.1 ± 1.5 s^{-1} (± 95% CI; Fig. 5B). This agreement is consistent with tight coupling between ATP hydrolysis and stepping. However, the data are also consistent with the motor sharing time between a diffusive state with no ATPase and bidirectional stepping state with an elevated ATPase rate. In contrast, Cin8$_{+28NC}$Kin had a mean plus-end velocity of 23.9 ± 6.9 nm/s on bovine microtubules (Fig. 2E), corresponding to 3 steps/s, and a k_{cat} of 6.9 ± 2.3 s^{-1} (± 95% CI). The ~two-fold faster ATPase rate for Cin8$_{+28NC}$Kin compared to its stepping rate suggests that instability of the native Cin8 neck coil leads to uncoupling between stepping and hydrolysis. This uncoupling also suggests that the greater proportion of undirected movement for Cin8$_{+28NC}$Kin (Fig. 2 & 3) results from bidirectional stepping and not from enhanced diffusion.

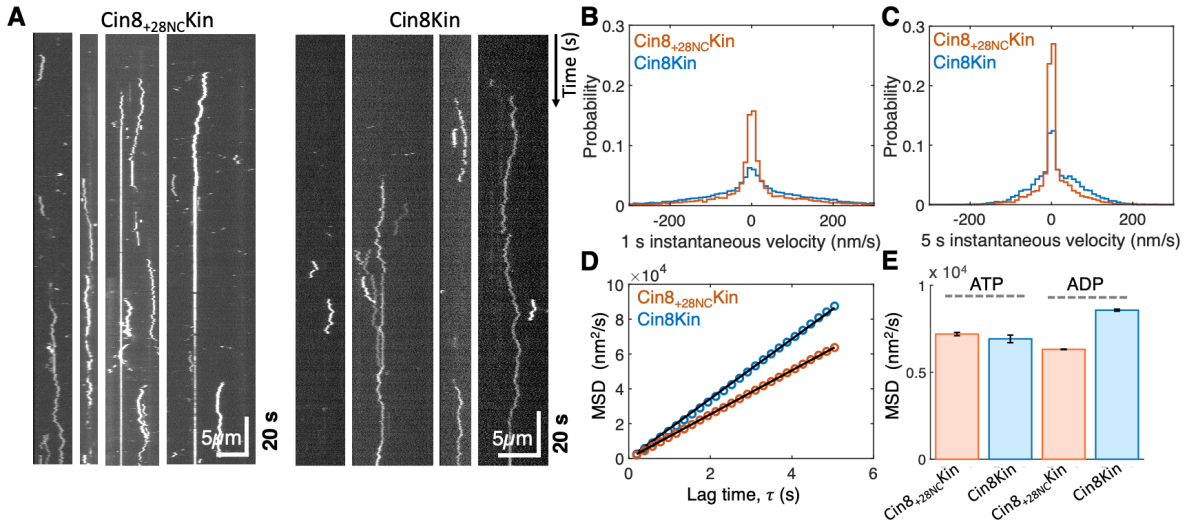

Fig. 6. Cin8 remains bound to microtubules in the presence of ADP. (A) Representative kymographs in the presence of 1 mM ADP on yeast microtubules. **(B)** 1 s and **(C)** 5 s instantaneous velocity distributions for Cin8$_{+28NC}$Kin (orange) and Cin8Kin (blue). **(D)** Mean squared displacement (MSD) comparison in ADP. Data were fit to MSD = 2Dτ, yielding D = 6314 ± 17 nm^2/s for Cin8$_{+28NC}$Kin and 8565 ± 58 nm^2/s for Cin8Kin (fit ± 95% CI). **(E)** Comparison of apparent diffusion coefficients for Cin8$_{+28NC}$Kin and Cin8Kin in ATP and ADP on yeast microtubules.

Cin8 dimers diffuse on MTs for long durations in the ADP-bound state

In a further effort to separate out thermally-driven diffusion from bidirectional stepping, we examined the behavior of the Cin8 dimers on yeast microtubules in the presence of 1 mM ADP, which generates a diffusive weak-binding state. Unlike most kinesins, which bind weakly to microtubules in ADP (28,44,45), Cin8 tetramers have been shown to bind for long durations in ADP (3,23,25,26). We found that both Cin8 dimers remained bound to microtubules for long durations in ADP (Fig. 6A). Thus, consistent with previous observations (24), Cin8 motor domains have inherently high microtubule affinity in ADP independent of their tetrameric structure or their tail domains.

To quantify motor diffusion in the ADP-bound state, we plotted the instantaneous velocity distributions for both motors and carried out a mean squared displacement (MSD) analysis. Both 1 s and 5 s instantaneous velocity distributions are centered around zero, as expected, indicating that directional motility is ATP hydrolysis-dependent (Fig. 6B&C). The apparent diffusion constants in ADP were 6314 ± 17 nm^2/s for $Cin8_{+28NC}Kin$ and 8565 nm^2/s ± 58 nm^2/s Cin8Kin (fit ± 95% CI; Fig. 6D&E), which are in the same range of the corresponding diffusion constants in ATP on yeast microtubules (Fig. 6E). Thus, the data don't exclude the possibility that the nondirected movements in ATP are 1D diffusion of the motors during phases when the motors are not stepping.

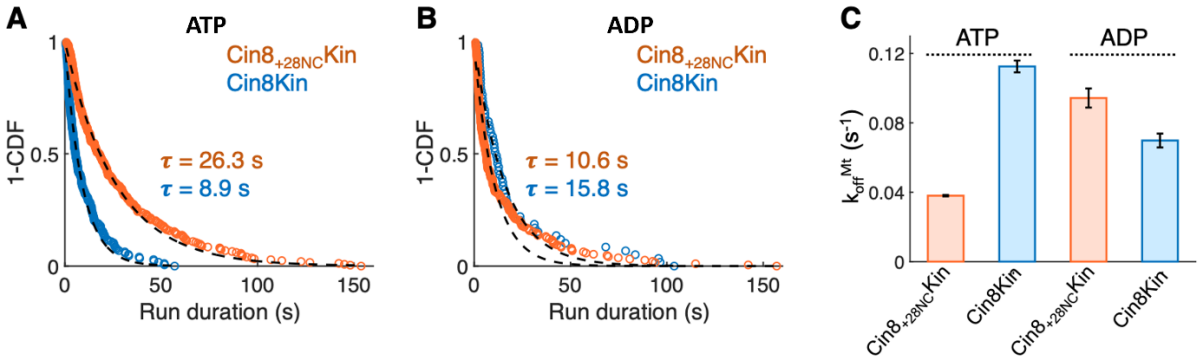

Fig. 5. Microtubule binding durations of Cin8 dimers on yeast microtubules. Distribution of bound durations (τ) from single-molecule motility traces of $Cin8_{+28NC}Kin$ and Cin8Kin in **(A)** ATP and **(B)** ADP. Data are plotted as 1 - Cumulative distribution function (1-CDF) and fit with an exponential (black lines). **(C)** Comparison of microtubule detachment rates (k_{off}^{Mt}), calculated as $k_{off}^{Mt} = 1/\tau$. Sample sizes (n) for $Cin8_{+28NC}Kin$ were 246 (ATP) and 190 (ADP); for Cin8Kin, 172 (ATP) and 59 (ADP). Error bars represent 95% CI. Processive and diffusive traces in ATP were analyzed separately and found to have similar binding durations (Fig. S6).

Cin8 neck-coil domain enhances microtubule binding duration in ATP but not ADP

To investigate the influence of inter-head tension on the overall microtubule affinity of Cin8$_{+28NC}$Kin and Cin8Kin, we quantified the residence times of Cin8 dimers in ATP and ADP on yeast microtubules. If flexibility of the Cin8 neck-coil reduces inter-head coordination needed for processive stepping, then Cin8$_{+28NC}$Kin should have shorter binding durations than Cin8Kin. In contrast, if flexibility of the Cin8 neck-coil reduces steric constraints and allows both heads to bind to the microtubule more readily, then Cin8$_{+28NC}$Kin should have longer binding durations than Cin8Kin. Mean binding durations in ATP were calculated by fitting an exponential function to the distribution of run durations. We found that Cin8$_{+28NC}$Kin remained bound to microtubules ~3-fold longer than Cin8Kin (26.3 ± 0.32 s and 8.9 ± 0.27 s, respectively (fit ± 95% CI); Fig. 7A). Thus, the data are consistent with flexibility of the Cin8 neck coil reducing steric constraints between the two heads and promoting a two-head binding state in ATP. To test whether similar behavior occurs in ADP, we repeated the analysis in 1 mM ADP and found the opposite result, with the Cin8$_{+28NC}$Kin binding duration (10.6 ± 0.61 s) being shorter than that for Cin8Kin (15.8 ± 0.67 s; Fig. 7B & C). Thus, in ATP the proximal Cin8 neck domain prolongs the microtubule binding duration in ATP, whereas in ADP it shortens the binding duration.

Discussion

For transport kinesins, processivity relies on mechanochemical coordination between the two motor domains; however, the degree to which the two heads of Cin8 are coordinated and whether this coordination plays a role in the bidirectional motility of Cin8 are not clear. We find that engineered Cin8 dimers move with a plus-end bias and exhibit undirected movements that result from a combination of ATP-driven bidirectional stepping and thermally-driven diffusion. Including the native neck-coil of Cin8 leads to more undirected movements and a slower net plus-end speed, no change in the ATP turnover rate, and a longer residence time on the microtubule. On yeast microtubules, Cin8 moved at a similar speeds as on bovine microtubules but with fewer undirected movements. These results suggest that plus-ended movement of Cin8 requires little coordination between the activities of its motor domains and instead relies on the high affinity of Cin8 in the ADP state.

Cin8 dimer motility is consistent with previous work

Motility of the two Cin8 dimer variants studied here is broadly consistent with previous work. Duselder et al constructed a Cin8Kin containing the full N-terminal, 4 residues more in the neck domain, and a shorter kinesin-1 dimerization domain (24). On

535 porcine microtubules in BRB80 buffer without added salt, the dimer showed bidirectional
536 movements with a small plus-ended mean velocity (18 nm/s) and an MSD exponent of 1.24
537 consistent with directional movements. Our Cin8Kin dimer had a faster net velocity (62
538 nm/s on bovine microtubules from Fig. 2E), a slightly higher MSD exponent of 1.38, and
539 clear plus-end directed segments not observed in that work. Although there are differences
540 in the motility analysis between the two studies, differences in the truncation points of the
541 constructs are the most likely explanation for the differences in motility. Consistent with
542 this, previous work using dimers having the same motor domain length as our Cin8Kin (38-
543 530) with a different dimerization strategy found similar plus-end gliding velocities in multi-
544 motor gliding assays (25). One consistent result from these dimer studies was that the fast
545 minus-end motility seen in Cin8 tetramers was absent, consistent with regions outside the
546 motor domain being required for fast minus-end velocities seen in tetramers.

547 **Diffusion and bidirectional stepping are not easily separated**

548 Because bidirectional stepping is a form of a random walk and random walks
549 inherently generate diffusion-like behavior (46), it is challenging to separate out
550 contributions of ATP-driven bidirectional stepping from simple thermally-driven diffusion.
551 The first argument in favor of bidirectional stepping is the substantial fraction of minus-end
552 velocity segments in the instantaneous velocity distributions (Fig. 2E and 3E). When we
553 analyzed whether a model consisting of plus-ended stepping together with thermal
554 diffusion could recapitulate the instantaneous velocity histograms, we failed to find a
555 diffusion constant that matched both the height of the velocity peak and the width of the
556 overall distribution. Although we can't rule out the possibility that more complex stepping
557 and diffusion models could better match the data, our analysis argues against diffusion
558 alone accounting for the undirected motility.

559 The second argument supporting bidirectional stepping is the fit of a three-
560 component Gaussian Mixture Model to the instantaneous velocity histograms (Fig. 4A). In
561 all cases the fits included a dominant peak (roughly half of the total) centered around the
562 mean plus-end velocity, consistent with active stepping. There was also a peak near zero
563 (~20-25% of total), consistent with thermally-driven diffusion. The third peak was broad
564 and centered at a positive velocity, properties consistent with it representing bidirectional
565 stepping with a plus-end bias. The fact that this broad peak represented 34% of the data for
566 $Cin8_{+28NC}$Kin but only 24% for Cin8Kin is consistent with the native Cin8 neck coil leading to
567 more bidirectional stepping.

568 The third argument supporting bidirectional stepping as the dominant source of
569 undirected movement is the relationship of the motor velocities to their ATPase rates. For
570 Cin8Kin, the ATPase rate (k_{cat} of 5 s^{-1}) was similar to the net stepping rate calculated from

571 the mean velocity (7 s^{-1}). This match could be interpreted as ATP hydrolysis being tightly
572 coupled to forward stepping; however, the substantial undirected movements suggest a
573 more complicated picture involving some combination of bidirectional stepping and
574 diffusion. The more important result was that the k_{cat} of $Cin8_{+28NC}$Kin (7 s^{-1}) was more than
575 twice the net stepping rate (3 s^{-1}). This discrepancy suggests that the observed net velocity
576 results from a combination ATP-driven plus- and minus-end directed steps. For instance, if
577 one ATP was associated with every step, the results could be explained by a model with a 5
578 s^{-1} plus-end stepping rate and a 2 s^{-1} minus-end stepping rate. However, the undirected
579 movements we observed, which lasted for multiple seconds for some motors and the
580 entire duration for a subset of motors, suggest that the Cin8 dimers alternate between
581 phases of ATP-driven stepping and thermally-driven diffusion where little or no stepping
582 occurs. In this case, diffusive periods with zero ATPase could be balanced by periods of
583 bidirectional stepping at rates substantially above the average.

584 Two pieces of evidence argue that at least some portion of the undirected
585 movements are due to thermally-driven diffusion. The first is that comparing the behavior
586 in ATP versus ADP, both the apparent diffusion constants and the microtubule off-rates
587 differ very little (Fig. 6E and 7C). Because the ADP state is generally the lowest affinity state
588 in the kinesin ATP hydrolysis cycle (44,47), both the diffusion constant and the dissociation
589 rate would be expected to be highest in ADP. One interpretation is that Cin8 spends most of
590 its ATP hydrolysis cycle in the ADP state, similar to what has been suggested for the
591 superprocessive kinesin-3 motor, KIF1A (28,48). Unfortunately, the high affinity of Cin8 for
592 mant-ADP (Fig. S7) prevented us from measuring the ADP off-rate directly. The second
593 argument that diffusion makes up part of the undirected movement is the different
594 behaviors on yeast versus bovine microtubules. Consistent with the general conservation
595 of tubulin from fungi to mammals, the mean velocities observed on the two substrates
596 were similar for both motors. However, there were more undirected movements on bovine
597 microtubules than on yeast microtubules, particularly for Cin8Kin. Motor landing rates
598 were also higher on bovine microtubules. We tentatively interpret the enhanced undirected
599 movements on bovine microtubules as resulting from more electrostatic interactions
600 between Cin8 and the bovine C-terminal tails, which shift the motor from a stepping state
601 to a diffusive state. The importance of the C-terminal tail to Cin8 motility was
602 demonstrated by a recent study that found that deleting the yeast β-tubulin C-terminal tail
603 reduces the on-rate, run length and velocity of full-length Cin8 (40).

604 **Cin8 lacks tight inter-head coordination**

605 In contrast to kinesin-1 where processivity is achieved by tight coordination between
606 the mechanochemical cycles of the two heads, we favor a model for Cin8 in which there is

607 little inter-head coordination and processivity is instead achieved by the inherent high
608 affinity of the motor domains for the microtubule. We found that in the presence of ADP,
609 Cin8 dimers bound to microtubules for long durations, consistent with previous
610 observations for tetrameric, dimeric, and monomeric Cin8 (3-5,24,25). This property differs
611 from the relatively fast microtubule off-rate of kinesin-1 in ADP state (44), and it relieves the
612 constraint inherent in kinesin-1 that the mechanochemical cycles of the heads remain out
613 of phase to minimize time in the ADP state (16). Notably, we found that Cin8$_{+28NC}$Kin moved
614 at a slower mean velocity than Cin8Kin and had more undirected motility, but it remained
615 bound to the microtubule nearly three-fold longer than Cin8Kin (Fig. 7A). We interpret this
616 to mean that the relative instability of the native Cin8 neck-coil domain diminishes
617 mechanical coupling between the two motor domains, resulting in Cin8$_{+28NC}$Kin spending a
618 greater fraction of time in the two-heads-bound state than Cin8Kin. It was shown
619 previously that disrupting the mechanical connection between the two heads of kinesin-1
620 by inserting six or more residues into the neck linker domain resulted in significant
621 backstepping under hindering loads, longer residence times under no load, and the motor
622 losing the requirement of ATP binding to occupy the two-heads-bound state (21,22). Thus,
623 there is precedence for a loosening of the mechanical connection between the two heads
624 of kinesin enabling the two-head-bound state.

625 Further evidence supporting a lack of interhead coupling in Cin8 come from
626 comparisons of our dimers to previous work on Cin8 monomers. It was found previously
627 that in multimotor gliding assays, monomeric Cin8 motor domains (residues 1-528 linked
628 to gelsolin for surface immobilization) moved microtubules at 20-40 nm/s, similar to our
629 gliding speeds for dimeric Cin8$_{+28NC}$Kin (Fig. 1) (49). Furthermore, in ATPase assays Cin8
630 monomers (residues 38-530) were found to have a k_{cat} of 4.1 s^{-1} (25), which is roughly half of
631 our dimer ATPase rates (meaning the rates are the same on a per-head basis). Thus,
632 multimotor gliding speeds and ATPase rates appear to be equivalent whether the heads are
633 connected through the Cin8 neck-coil or not. Notably, in Cin8Kin where we connected two
634 Cin8 heads directly through the stable kinesin-1 neck-coil domain, the motor moved faster
635 and with more plus-end directionality than when the Cin8 neck-coil was present. These
636 results suggest that features that regulate Cin8 directionality, such as the tail domain (24),
637 N-terminal extension (26), loop-8 (25) and phosphorylation (50,51) could exert their effects
638 by altering inter-head coordination. Similarly, geometries that promote plus-end
639 directionality such as motor clustering (4,23) and crosslinking of antiparallel microtubules
640 (3,10) could be thought of as mechanically coordinating the motor domains.

641

Author contributions

H.P., W.O.H. and L.G. developed original ideas for the project. H.P. and W.O.H. designed research. H.P. and T-C.M. carried out experiments and analyzed data. T-C.M. carried out simulations. H.P., T-C.M., L.G. and W.O.H. interpreted data. E.B. and L.M.R. generated yeast tubulin and helped design experiments. H.P. and W.O.H. wrote the manuscript and all authors edited the manuscript.

Declaration of interests

The authors declare no competing interests.

Acknowledgments

This work was funded by NIH R35 GM139568 awarded to W.O.H., NIH R35 GM156385 awarded to L.M.R., and ISF grant 629/23 awarded to L.G. The authors thank members of the Hancock and Gheber labs for helpful suggestions.

References

1. Henningsen, U., and Schliwa, M. (1997) Reversal in the direction of movement of a molecular motor. *Nature* **389**, 93-96
2. Endow, S. A., and Waligora, K. W. (1998) Determinants of kinesin motor polarity. *Science* **281**, 1200-1202
3. Gerson-Gurwitz, A., Thiede, C., Movshovich, N., Fridman, V., Podolskaya, M., Danieli, T., Lakamper, S., Klopfenstein, D. R., Schmidt, C. F., and Gheber, L. (2011) Directionality of individual kinesin-5 Cin8 motors is modulated by loop 8, ionic strength and microtubule geometry. *EMBO J* **30**, 4942-4954
4. Roostalu, J., Hentrich, C., Bieling, P., Telley, I. A., Schiebel, E., and Surrey, T. (2011) Directional switching of the kinesin Cin8 through motor coupling. *Science* **332**, 94-99
5. Fridman, V., Gerson-Gurwitz, A., Shapira, O., Movshovich, N., Lakamper, S., Schmidt, C. F., and Gheber, L. (2013) Kinesin-5 Kip1 is a bi-directional motor that stabilizes microtubules and tracks their plus-ends in vivo. *J Cell Sci* **126**, 4147-4159
6. Endow, S. A., and Higuchi, H. (2000) A mutant of the motor protein kinesin that moves in both directions on microtubules. *Nature* **406**, 913-916
7. Popchock, A. R., Tseng, K. F., Wang, P., Karplus, P. A., Xiang, X., and Qiu, W. (2017) The mitotic kinesin-14 KlpA contains a context-dependent directionality switch. *Nature communications* **8**, 13999

677 8. Mann, B. J., and Wadsworth, P. (2019) Kinesin-5 Regulation and Function in Mitosis.
678 *Trends Cell Biol* **29**, 66-79
679 9. Pandey, H., Popov, M., Goldstein-Levitin, A., and Gheber, L. (2021) Mechanisms by
680 Which Kinesin-5 Motors Perform Their Multiple Intracellular Functions. *Int J Mol Sci*
681 **22**
682 10. Shapira, O., Goldstein, A., Al-Bassam, J., and Gheber, L. (2017) A potential
683 physiological role for bi-directional motility and motor clustering of mitotic kinesin-5
684 Cin8 in yeast mitosis. *J Cell Sci* **130**, 725-734
685 11. Britto, M., Goulet, A., Rizvi, S., von Loeffelholz, O., Moores, C. A., and Cross, R. A.
686 (2016) Schizosaccharomyces pombe kinesin-5 switches direction using a steric
687 blocking mechanism. *Proc Natl Acad Sci U S A* **113**, E7483-E7489
688 12. Rice, S., Lin, A. W., Safer, D., Hart, C. L., Naber, N., Carragher, B. O., Cain, S. M.,
689 Pechatnikova, E., Wilson-Kubalek, E. M., Whittaker, M., Pate, E., Cooke, R., Taylor, E.
690 W., Milligan, R. A., and Vale, R. D. (1999) A structural change in the kinesin motor
691 protein that drives motility. *Nature* **402**, 778-784
692 13. Vale, R. D., and Milligan, R. A. (2000) The way things move: looking under the hood of
693 molecular motor proteins. *Science* **288**, 88-95
694 14. Hwang, W., Lang, M. J., and Karplus, M. (2008) Force generation in kinesin hinges on
695 cover-neck bundle formation. *Structure* **16**, 62-71
696 15. Khalil, A. S., Appleyard, D. C., Labno, A. K., Georges, A., Karplus, M., Belcher, A. M.,
697 Hwang, W., and Lang, M. J. (2008) Kinesin's cover-neck bundle folds forward to
698 generate force. *Proc Natl Acad Sci U S A* **105**, 19247-19252
699 16. Hancock, W. O. (2016) The Kinesin-1 Chemomechanical Cycle: Stepping Toward a
700 Consensus. *Biophys J* **110**, 1216-1225
701 17. Gennerich, A., and Vale, R. D. (2009) Walking the walk: how kinesin and dynein
702 coordinate their steps. *Curr Opin Cell Biol* **21**, 59-67
703 18. Shastry, S., and Hancock, W. O. (2011) Interhead tension determines processivity
704 across diverse N-terminal kinesins. *Proc Natl Acad Sci U S A* **108**, 16253-16258
705 19. Niitani, Y., Matsuzaki, K., Jonsson, E., Vale, R. D., and Tomishige, M. (2025) Kinetic
706 regulation of kinesin's two motor domains coordinates its stepping along
707 microtubules. *eLife* **14**
708 20. Shastry, S., and Hancock, W. O. (2010) Neck linker length determines the degree of
709 processivity in Kinesin-1 and Kinesin-2 motors. *Current Biology* **20**, 939-943
710 21. Yildiz, A., Tomishige, M., Gennerich, A., and Vale, R. D. (2008) Intramolecular strain
711 coordinates kinesin stepping behavior along microtubules. *Cell* **134**, 1030-1041
712 22. Clancy, B. E., Behnke-Parks, W. M., Andreasson, J. O., Rosenfeld, S. S., and Block, S.
713 M. (2011) A universal pathway for kinesin stepping. *Nat Struct Mol Biol* **18**, 1020-
714 1027
715 23. Pandey, H., Reithmann, E., Goldstein-Levitin, A., Al-Bassam, J., Frey, E., and Gheber,
716 L. (2021) Drag-induced directionality switching of kinesin-5 Cin8 revealed by cluster-
717 motility analysis. *Sci Adv* **7**
718 24. Duselder, A., Fridman, V., Thiede, C., Wiesbaum, A., Goldstein, A., Klopfenstein, D.
719 R., Zaitseva, O., Janson, M. E., Gheber, L., and Schmidt, C. F. (2015) Deletion of the

720 Tail Domain of the Kinesin-5 Cin8 Affects Its Directionality. *J Biol Chem* **290**, 16841-
721 16850
722 25. Pandey, H., Singh, S. K., Sadan, M., Popov, M., Singh, M., Davidov, G., Inagaki, S., Al-
723 Bassam, J., Zarivach, R., Rosenfeld, S. S., and Gheber, L. (2021) Flexible microtubule
724 anchoring modulates the bi-directional motility of the kinesin-5 Cin8. *Cell Mol Life*
725 *Sci* **78**, 6051-6068
726 26. Singh, S. K., Siegler, N., Pandey, H., Yanir, N., Popov, M., Goldstein-Levitin, A.,
727 Sadan, M., Debs, G., Zarivach, R., Frank, G. A., Kass, I., Sindelar, C. V., Zalk, R., and
728 Gheber, L. (2024) Noncanonical interaction with microtubules via the N-terminal
729 nonmotor domain is critical for the functions of a bidirectional kinesin. *Sci Adv* **10**,
730 eadi1367
731 27. Mickolajczyk, K. J., Deffenbaugh, N. C., Ortega Arroyo, J., Andrecka, J., Kukura, P.,
732 and Hancock, W. O. (2015) Kinetics of nucleotide-dependent structural transitions
733 in the kinesin-1 hydrolysis cycle. *Proc Natl Acad Sci U S A* **112**, E7186-7193
734 28. Zaniewski, T. M., Gicking, A. M., Fricks, J., and Hancock, W. O. (2020) A kinetic
735 dissection of the fast and superprocessive kinesin-3 KIF1A reveals a predominant
736 one-head-bound state during its chemomechanical cycle. *J Biol Chem* **295**, 17889-
737 17903
738 29. Cleary, J. M., Kim, T., Cook, A. S. I., McCormick, L. A., Hancock, W. O., and Rice, L.
739 M. (2022) Measurements and simulations of microtubule growth imply strong
740 longitudinal interactions and reveal a role for GDP on the elongating end. *eLife* **11**,
741 e75931
742 30. Mahamdeh, M., Simmert, S., Luchniak, A., Schaffer, E., and Howard, J. (2018) Label-
743 free high-speed wide-field imaging of single microtubules using interference
744 reflection microscopy. *J Microsc* **272**, 60-66
745 31. Ruhnow, F., Zwicker, D., and Diez, S. (2011) Tracking single particles and elongated
746 filaments with nanometer precision. *Biophys J* **100**, 2820-2828
747 32. Schindelin, J., Arganda-Carreras, I., Frise, E., Kaynig, V., Longair, M., Pietzsch, T.,
748 Preibisch, S., Rueden, C., Saalfeld, S., Schmid, B., Tinevez, J. Y., White, D. J.,
749 Hartenstein, V., Eliceiri, K., Tomancak, P., and Cardona, A. (2012) Fiji: an open-
750 source platform for biological-image analysis. *Nat Methods* **9**, 676-682
751 33. Huang, T. G., and Hackney, D. D. (1994) Drosophila kinesin minimal motor domain
752 expressed in Escherichia coli. Purification and kinetic characterization. *J Biol Chem*
753 **269**, 16493-16501
754 34. Ohashi, K. G., Han, L., Mentley, B., Wang, J., Fricks, J., and Hancock, W. O. (2019)
755 Load-dependent detachment kinetics plays a key role in bidirectional cargo
756 transport by kinesin and dynein. *Traffic* **20**, 284-294
757 35. Ma, T. C., Gicking, A. M., Feng, Q., and Hancock, W. O. (2023) Simulations suggest
758 robust microtubule attachment of kinesin and dynein in antagonistic pairs. *Biophys*
759 *J* **122**, 3299-3313
760 36. Chen, Y., and Hancock, W. O. (2015) Kinesin-5 is a microtubule polymerase. *Nature*
761 *communications* **6**, 8160

37. Chen, G. Y., Mickolajczyk, K. J., and Hancock, W. O. (2016) The Kinesin-5 Chemomechanical Cycle Is Dominated by a Two-heads-bound State. *J Biol Chem* **291**, 20283-20294
38. Chen, G. Y., Cleary, J. M., Asenjo, A. B., Chen, Y., Mascaro, J. A., Arginteanu, D. F. J., Sosa, H., and Hancock, W. O. (2019) Kinesin-5 Promotes Microtubule Nucleation and Assembly by Stabilizing a Lattice-Competent Conformation of Tubulin. *Curr Biol* **29**, 2259-2269 e2254
39. Tripet, B., Vale, R. D., and Hodges, R. S. (1997) Demonstration of coiled-coil interactions within the kinesin neck region using synthetic peptides. Implications for motor activity. *J Biol Chem* **272**, 8946-8956
40. Thomas, E. C., and Moore, J. K. (2025) Selective regulation of kinesin-5 function by beta-tubulin carboxy-terminal tails. *J Cell Biol* **224**
41. Coy, D. L., Wagenbach, M., and Howard, J. (1999) Kinesin takes one 8-nm step for each ATP that it hydrolyzes. *J Biol Chem* **274**, 3667-3671
42. Schnitzer, M. J., and Block, S. M. (1997) Kinesin hydrolyses one ATP per 8-nm step. *Nature* **388**, 386-390
43. Okada, Y., and Hirokawa, N. (2000) Mechanism of the single-headed processivity: diffusional anchoring between the K-loop of kinesin and the C terminus of tubulin. *Proc Natl Acad Sci U S A* **97**, 640-645
44. Hancock, W. O., and Howard, J. (1999) Kinesin's processivity results from mechanical and chemical coordination between the ATP hydrolysis cycles of the two motor domains. *Proc Natl Acad Sci U S A* **96**, 13147-13152
45. Chen, G. Y., Arginteanu, D. F., and Hancock, W. O. (2015) Processivity of the kinesin-2 KIF3A results from rear head gating and not front head gating. *J Biol Chem* **290**, 10274-10294
46. Berg, H. C. (1993) *Random Walks in Biology*, 2nd ed., Princeton University Press, Princeton, NJ
47. Romberg, L., and Vale, R. D. (1993) Chemomechanical cycle of kinesin differs from that of myosin. *Nature* **361**, 168-170
48. Zaniewski, T. M., and Hancock, W. O. (2023) Positive charge in the K-loop of the kinesin-3 motor KIF1A regulates superprocessivity by enhancing microtubule affinity in the one-head-bound state. *J Biol Chem* **299**, 102818
49. Yamagishi, M., Maruyama, Y., Sugawa, M., and Yajima, J. (2021) Characterization of the motility of monomeric kinesin-5/Cin8. *Biochem Biophys Res Commun* **555**, 115-120
50. Avunie-Masala, R., Movshovich, N., Nissenkorn, Y., Gerson-Gurwitz, A., Fridman, V., Koivomagi, M., Loog, M., Hoyt, M. A., Zaritsky, A., and Gheber, L. (2011) Phospho-regulation of kinesin-5 during anaphase spindle elongation. *J Cell Sci* **124**, 873-878
51. Shapira, O., and Gheber, L. (2016) Motile properties of the bi-directional kinesin-5 Cin8 are affected by phosphorylation in its motor domain. *Sci Rep* **6**, 25597

Supporting information

Dimeric Cin8 motors have an inherent plus-end bias and weak inter-head coordination

Running title: Cin8 dimer motility

Himanshu Pandey[1], Tzu-Chen Ma[1], Eric Bonventre[2], Luke M. Rice[2], Larisa Gheber[3], and William O. Hancock[1,4 *]

[1] Department of Biomedical Engineering, Pennsylvania State University, University Park, Pennsylvania, USA
[2] Department of Biophysics, University of Texas Southwestern Medical Center, Dallas, Texas, USA
[3] Department of Chemistry, Ben-Gurion University of the Negev, Israel
[4] Department of Chemistry, Pennsylvania State University, University Park, Pennsylvania, USA

* Corresponding author:
William O. Hancock
Email: woh1@psu.edu

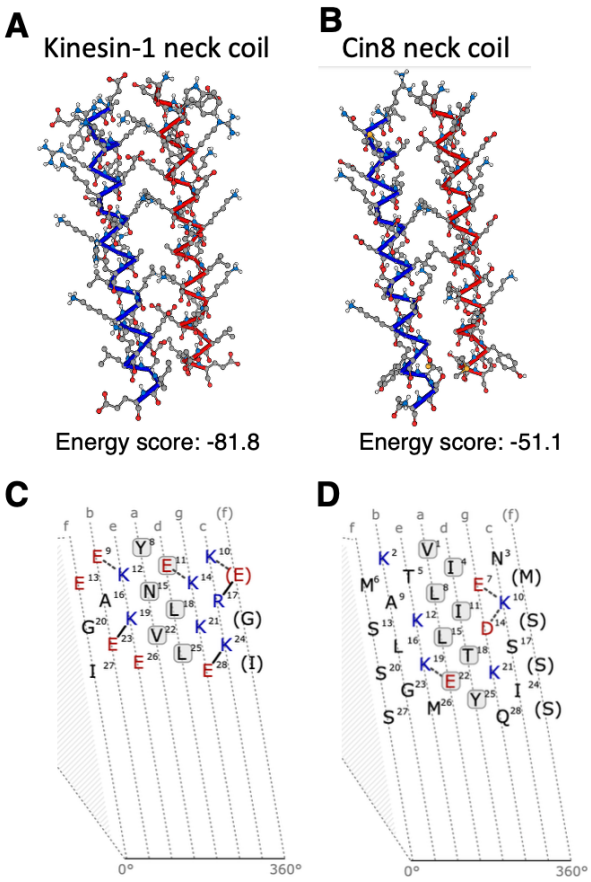

Fig. S1. Cin8 is predicted to have a less stable neck coiled-coil than kinesin-1. (A, B) Coiled-coil prediction models for the proximal neck coil domains of kinesin-1 (A) and Cin8 (B) generated using CCbuilder 2.0 (1). The predicted coiled-coil stability scores were −81.8 for kinesin-1 and −51.1 for Cin8, with more negative values indicating greater stability. The backbones of the interacting helices are shown in blue and red, with side chains depicted in grey. **(C, D)** Predicted stabilizing interactions within the coiled-coil domains of kinesin-1 (C) and Cin8 (D). For kinesin-1, three strong (solid lines) and three intermediate (dashed lines) stabilizing interactions were identified, whereas only three intermediate interactions were predicted for Cin8. Coiled-coil predictions and alignment were performed using CCbuilder 2.0, COcoNat (2), T-Coffee (3), and Waggawagga (4).

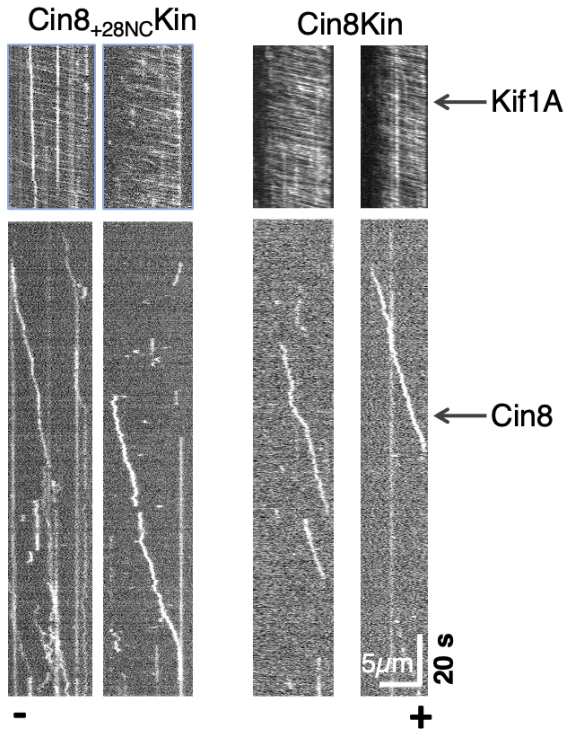

Fig. S2: Microtubule polarity dermination. To define microtubule polarity, fluorescent KIF1A (5) was introduced at the end of the experiment (top). Kymographs at bottom are same microtubule showing Qdot-labeled Cin8$_{+28NC}$Kin or Cin8Kin motility, with microtubule polarity marked at the bottom of kymograph.

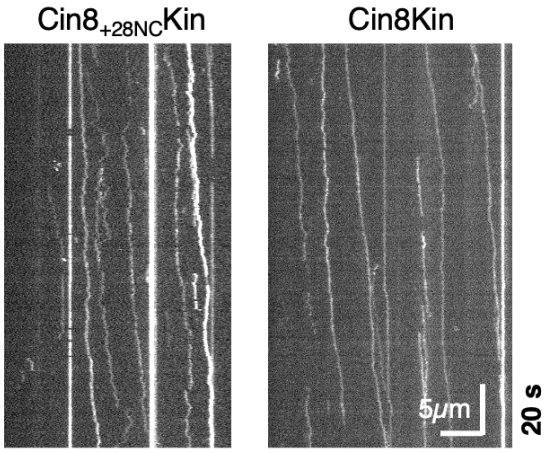

Fig. S3: Single-molecule motility of Cin8 dimers on bovine microtubules in BRB80 buffer plus 110 mM KCl. Net plus-end motility was retained even at elevated ionic strength with whole trace velocities of 47.3 ± 7.0 and 84.1 ± 7.6 nm/s for Cin8$_{+28NC}$Kin (n = 27) and Cin8Kin (n = 30), respectively (mean ± SEM).

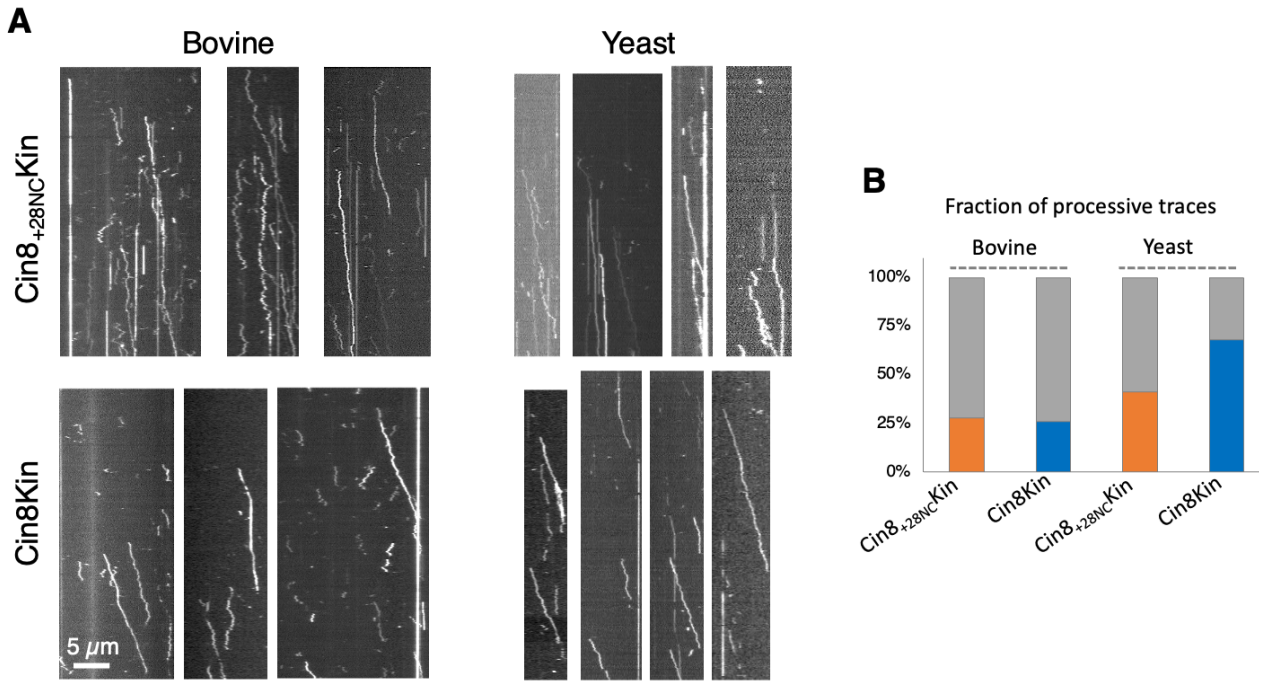

Fig. S4: Comparison of Cin8 dimer motility on bovine and yeast microtubules. (A) Representative kymographs for Cin8$_{+28NC}$Kin and Cin8Kin motility on bovine or yeast microtubules as indicated at the top. On yeast microtubules Cin8 dimers move with more consistent plus-end directionality. **(B)** Fraction of processive traces for each condition, defined as traces with overall velocity >20 nm/s and overall displacement >1 μm. The grey area at the top of each bar represents fraction of motors with undirected motility.

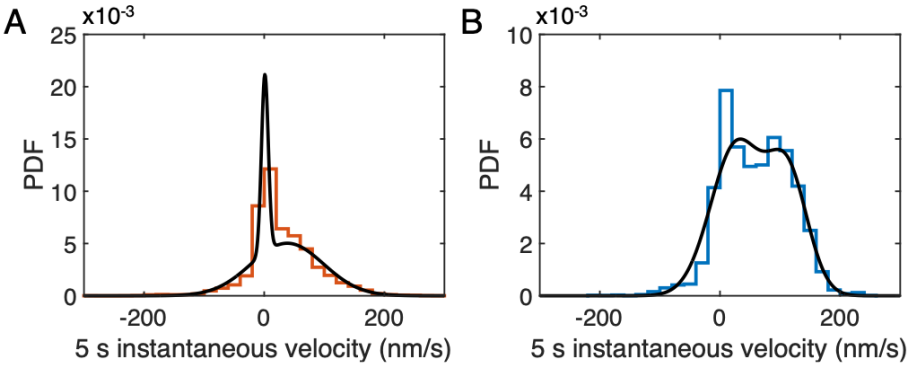

Fig. S5. Velocity distributions for Cin8$_{+28NC}$Kin (A) and Cin8Kin (B) could not be fit well by the sum of two Gaussians. The velocity distributions are depicted in orange (Cin8$_{+28NC}$Kin) or blue (Cin8Kin) and the Gaussian Mixture Model (GMM) fit in black. The Bayesian Information Criterion (BIC) of 3-Gaussian and 2-Gaussian models for Cin8$_{+28NC}$Kin are $1.0132*10^5$ and $1.0180*10^5$, respectively. For Cin8Kin, the BIC of 3-Gaussian and 2-Gaussian models are $9.2865*10^4$ and $9.3623*10^4$, respectively. These results suggest that the distributions are better explained by three Gaussians.

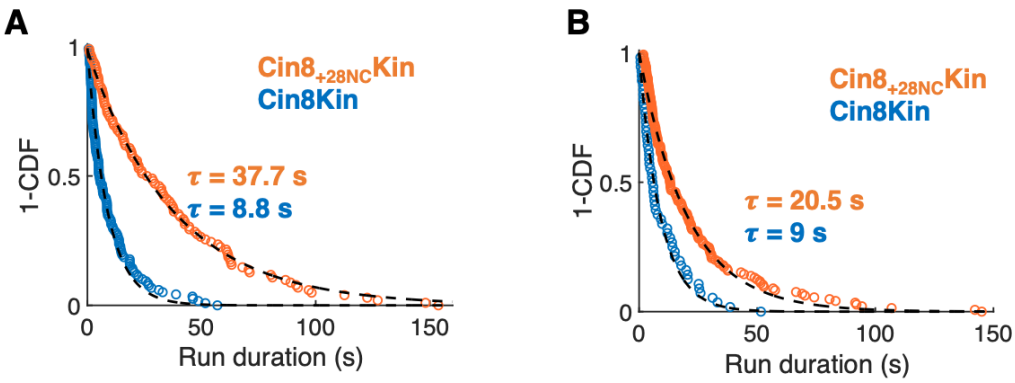

Fig. S6. Microtubule binding durations of processive and undirected Cin8 dimers on yeast microtubules in ATP. Processive molecules were defined as those with average velocities >20 nm/s and net displacements >1 µm. Cumulative distribution functions (1- CDF) of run durations for **(A)** processive and **(B)** undirected motility traces for Cin8$_{+28NC}$Kin and Cin8Kin were fit by single exponential functions to obtain the mean run duration, τ, for each.

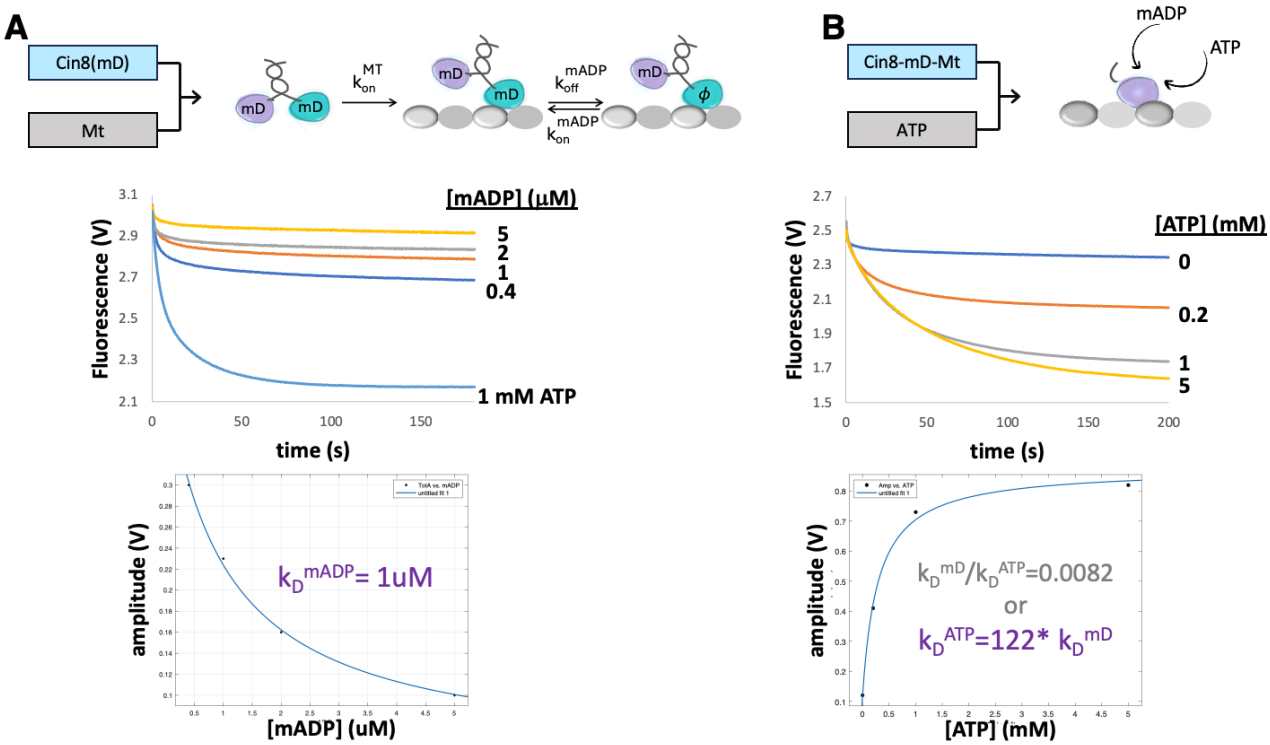

Fig. S7. Cin8 has a high affinity for mant-ADP. (A) To measure microtubule-stimulated mant-ADP release, mant-ADP labeled Cin8Kin dimers were flushed against microtubules in the presence of varying concentrations of free mant-ADP. Experiments were carried out at 21 °C in BRB80 buffer using an Applied Photophysics SX20 spectrofluorometer at 356-nm excitation with a 395 long-pass emission filter. The conditions in the chamber are 5 µM microtubules, 0.2 µM Cin8, and mADP or

ATP as noted. Note that the fall in fluorescence, corresponding to mantADP release is small and concentration dependent, denoting incomplete mantADP release. Full mantADP release was achieved by flushing mADP labelled motors against 5 μM microtubules + 1 mM ATP (chamber concentrations). To determine the mantADP affinity of microtubule-bound Cin8, the fall in the fluorescence amplitude was plotted against the free mant-ADP concentration and fit using $\mathrm{f(mADP)} = \mathrm{A} * \left(1 - \frac{[\mathrm{mADP}]}{[\mathrm{mADP}]+\mathrm{K_D}}\right) + \mathrm{c}$, where A is the maximum amplitude, c is an offset, and K_D is the dissociation constant. The fit estimated K_D^{mADP} = 1 μM for microtubule-bound Cin8. **(B)** A competition assay between mant-ADP and ATP in the absence of microtubules was performed by flushing microtubule-bound mant-ADP labeled Cin8 monomer against varying concentrations of ATP. The amplitude of the fall in fluorescence is plotted against [ATP] and fit using $\mathrm{f(ATP)} = \mathrm{A} * \left(1 - \frac{[\mathrm{mADP}]}{[\mathrm{mADP}]+\frac{K_D^{mADP}}{K_D^{ATP}}*[ATP]}\right) + \mathrm{c}$, where A is the maximum amplitude and c is the offset. The resulting fit gave $K_D^{ATP} = 122 * K_D^{mant-ADP}$. Thus, the affinity for mantADP is 122 times tighter than the affinity for ATP. This complicates mantADP stopped flow experiments with Cin8.

Fit:	**Bovine MTs**			**Yeast MTs**		
MSD = aτ$^{\alpha}$ + b	**a**	**α**	**b**	**a**	**α**	**b**
Cin8Kin	2.03*10^4 ±0.04*10^4	**1.38 ±0.01**	5034 ±550	1.16*10^4 ±0.03*10^4	**1.64 ±0.01**	1727 ±435
Cin8$_{+28NC}$Kin	2.15*10^4 ±0.04*10^4	**1.29 ±0.01**	2278 ±550	1.17*10^4 ±0.03*10^4	**1.29 ±0.01**	1844 ±323

Table S1. Fits to MSD results in Fig. 2F and 3F where α=1 represents diffusion and α=2 represents processive movement.

Supplementary references:

1. Wood, C. W., and D. N. Woolfson. 2018. CCBuilder 2.0: Powerful and accessible coiled-coil modeling. Protein Sci 27:103-111.
2. Madeo, G., C. Savojardo, M. Manfredi, P. L. Martelli, and R. Casadio. 2023. CoCoNat: a novel method based on deep learning for coiled-coil prediction. Bioinformatics 39.
3. Notredame, C., D. G. Higgins, and J. Heringa. 2000. T-Coffee: A novel method for fast and accurate multiple sequence alignment. J Mol Biol 302:205-217.
4. Simm, D., K. Hatje, and M. Kollmar. 2015. Waggawagga: comparative visualization of coiled-coil predictions and detection of stable single alpha-helices (SAH domains). Bioinformatics 31:767-769.
5. Zaniewski, T. M., A. M. Gicking, J. Fricks, and W. O. Hancock. 2020. A kinetic dissection of the fast and superprocessive kinesin-3 KIF1A reveals a predominant one-head-bound state during its chemomechanical cycle. J Biol Chem 295:17889-17903.